

URTeC: 2692030

## Recommendations From Error Analysis of Single-Well Microseismic Data With Full-wavefield Moment Tensor Inversion: A Case Study

Juan M. Lorenzo\*<sup>1</sup>, Trudy L. Watkins<sup>1</sup> Arash-Dahi Taleghani<sup>2</sup>

<sup>1</sup>Department of Geology and Geophysics, <sup>2</sup>Department of Petroleum Engineering, Louisiana State University.

Copyright 2017, Unconventional Resources Technology Conference (URTeC) DOI 10.15530-urtec-2017- 2692030  
This paper was prepared for presentation at the Unconventional Resources Technology Conference held in Austin, Texas, USA, 24-26 July 2017.

The URTeC Technical Program Committee accepted this presentation on the basis of information contained in an abstract submitted by the author(s). The contents of this paper have not been reviewed by URTeC and URTeC does not warrant the accuracy, reliability, or timeliness of any information herein. All information is the responsibility of, and, is subject to corrections by the author(s). Any person or entity that relies on any information obtained from this paper does so at their own risk. The information herein does not necessarily reflect any position of URTeC. Any reproduction, distribution, or storage of any part of this paper without the written consent of URTeC is prohibited.

### Summary

Microseismic events and their source mechanisms play a significant role in our understanding of hydraulic fracturing. To better identify the reliability of source mechanisms, we examine the limitations of microseismic field data imposed by (1) lack of angular coverage, (2) moment tensor inversion constraints, and (3) effects of mild anisotropy. We use synthetic seismograms to examine cases of either pure double-couple (DC) or compensated-linear-vector dipole (CLVD) sources. The open-source full-wavefield moment tensor inversion code (ISOLA) incorporates both near- and intermediate-field terms, which can increase the accuracy of the inversion if source-receiver distances are small. The tested locations and dominant source frequencies of the synthetic seismograms used for analysis resemble the expected locations and dominant frequencies of microseismic events extracted from a multi-stage field data set in the Barnett Shale of East Texas. We conclude that although a horizontal receiver array can provide greater angular coverage of vertical failure planes than a vertical receiver array, the strike of shear (DC) sources cannot be accurately resolved unless the receiver array has angular coverage to sample both sides of the shear failure plane. If the source is DC, the inversion can result in a CLVD mechanism that is overestimated by up to ~40% and if the source is CLVD, the DC mechanism can be overestimated by ~20%. Errors in the inversion results are interpreted to be because of the lack of receiver angular coverage of the source rather than possible errors associated with source mislocation. The use of the deviatoric assumption decreases the error in the resolved source mechanism by ~30-~40%, however, this increases the error in the resolved source strike to ~15°-~35°. For pure shear sources, 5% VTI anisotropy in the medium has minimal effect on source orientation (<15°) but can introduce 25-50 m of error in the source location. The neglect of anisotropy in moment tensor inversion has a greater effect (~40% variation) on the estimated source mechanism for pure CLVD sources than for pure DC sources.

### Introduction

Microseismic data analysis is subject to various sources of error. Data collected along vertical arrays of receivers suffer from lack of angular coverage so that estimations of both the source mechanism and its orientation are prone to errors (Eaton & Forouhdeh, 2011; Vavryčuk, 2007). A lack of accounting for possible anisotropy during inversion means that tensile mechanisms can be overestimated and fault planes misoriented (Sileny & Vavryčuk, 2002; Vavryčuk, 2005). Typically only far-field terms are considered and sources estimations are constrained in order to compensate for the lack of angular coverage (Vavryčuk, 2007; Warpinski & Du, 2010). Full-wavefield moment tensor inversion, which includes the intermediate- and near-field terms, can be used to increase the accuracy of the inversion results for microseismic data with small source-receiver distances (Song & Toksoz, 2011).

We aim to answer the following questions:

1. Can accurate source mechanisms be resolved from a single horizontal array of receivers using full-wavefield moment tensor inversion?
2. How does the angular coverage of an event affect the accuracy of the inversion?
3. How does the isotropic velocity model affect the results of the inversion for sources generated in an anisotropic medium?

Horizontal receiver arrays may provide better angular coverage than vertical receiver arrays if they can sample the seismic field on both sides of the vertical failure plane of a hydraulic fracture. Horizontal arrays proximal to the microseismic events may also detect the intermediate- and near-field components of the seismic field that could improve the quality of the moment tensor inversion. We expect that better angular coverage, should lead to less error in the moment tensor solution.

Hydraulic fracturing treatments are often completed in shale-rich formations whose seismic velocities can display some degree of anisotropy (Warpinski et al., 2009). An understanding of the error introduced by only assuming isotropy can aid our interpretations. A neglect of anisotropy in the moment tensor inversion should introduce errors into the event location and estimated mechanism percentages.

We address these issues using synthetic seismograms as the input microseismic data for moment tensor inversion. Synthetic seismograms provide the ideal scenario of noise-free data and the results of their inversion can be compared to the input parameters of the source in order to evaluate the possible causes of error in the moment tensor inversion. We calculate synthetic seismograms of body waves (P- and S-waves) with inputs of the source-receiver geometry, seismic velocities, dominant source frequency and moment tensor (Aki and Richards, 2002, p. 77). In order to provide some similarity between our model parameter and field conditions, we use source-receiver geometry, seismic velocities and geological conditions taken from a field case of hydraulic fracturing treatment (courtesy of Schlumberger) near a known fault zone in the Barnett Shale.

Overall, an estimate of the distribution of microseismic events may be sufficient to identify the extent of fracture growth and orientation during the treatment, fracture height and length, and the extent of the stimulated reservoir volume (van der Baan et al., 2013). As well, the extent of fracture growth aids in the analysis of the efficiency of the treatment by determining if fractures extend beyond the targeted zone of hydrocarbons (Eisner et al., 2006). However, additional estimations of the type of opening failure (source mechanism) can also contribute to evaluation of the effectiveness of the treatment (Urbancic et al., 2009; van der Baan et al., 2013).

## Theory and /or Method

### Moment Tensor

A moment tensor ( $M$ ) is the mathematical representation of the orientation of the fault plane and the type of failure (tensile and/or shearing) at the origin of an earthquake (Baig and Urbancic, 2010). The displacement  $u$  detected by a seismic receiver is a function of  $M$  and the Green's function  $G$  (Earth model):

$$u_n(x, t) = M_{pq} * G_{np,q} \quad (1)$$

where  $n$  is the  $n$ th component of displacement and  $p$  and  $q$  represent the coupled forces acting along the  $q$ -axis in  $p$  direction (Aki and Richards, 2002; Jost and Hermann, 1989) the  $M$  is written as the matrix:

$$M = \begin{bmatrix} M_{xx} & M_{xy} & M_{xz} \\ M_{yx} & M_{yy} & M_{yz} \\ M_{zx} & M_{zy} & M_{zz} \end{bmatrix} \quad (2)$$

and is symmetric ( $M_{xy} = M_{yx}$ ,  $M_{xz} = M_{zx}$ , and  $M_{yz} = M_{zy}$ ) (Fig. 1) in order to conserve angular momentum (Forouhideh and Eaton, 2009).

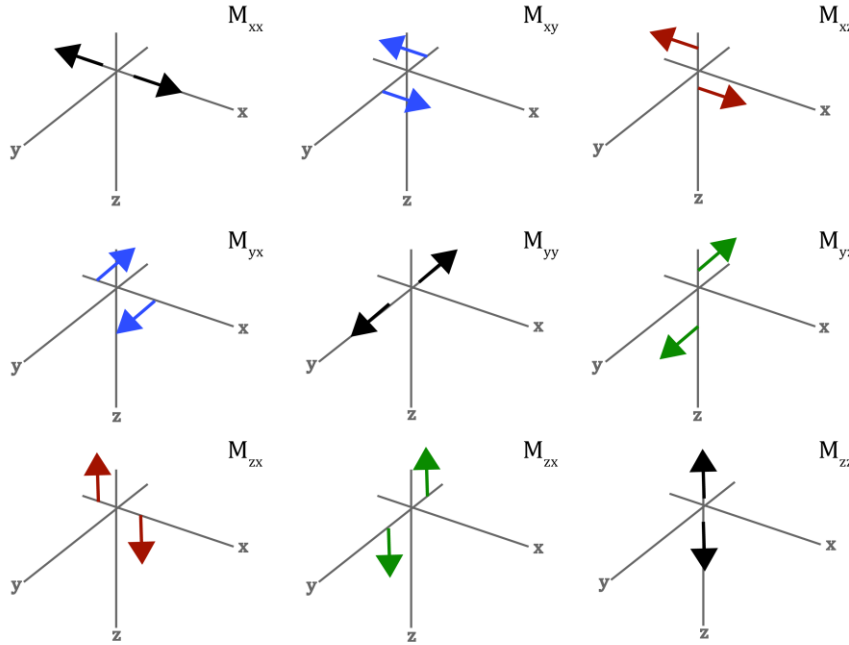


**Figure 1** Moment tensor  $M$  represents the nine double-couples of force acting at a source (adapted from Jost and Hermann (1989)). Because  $M$  is symmetric,  $M_{xy}=M_{yx}$  (blue),  $M_{xz}=M_{zx}$  (red), and  $M_{yz}=M_{zy}$  (green) (Forouhdeh and Eaton, 2009). The double-couple forces along the diagonal of  $M$  ( $M_{xx}$ ,  $M_{yy}$ , and  $M_{zz}$ , black) represent a volumetric change at the source (Stein and Wysession, 2003).

The DC (double-couple) component represents shearing at the source such as fault slip. Shearing can occur as strike-slip (in direction of strike) or dip-slip (in direction of dip) movement (Stein and Wysession, 2003). The radiation pattern of the DC source is symmetric about the origin of the source (Fig. 2). The plane perpendicular to the fault plane is called the auxiliary plane (i.e., the W-E line in the beach-ball diagram for the DC source in Figure 2--Bormann et al., 2013). The CLVD (compensated linear vector dipole) component indicates crack opening or closing (Baig and Urbancic, 2010; Stein and Wysession, 2003). The third component is the ISO (isotropic) component that represents volumetric change. A positive ISO component is an explosive event whereas a negative ISO component is an implosive event (Baig and Urbancic, 2010).

To interpret the DC, CLVD, and ISO mechanisms from moment tensors, the tensors are decomposed mathematically into an ISO tensor ( $M_{ISO}$ ) and a deviatoric tensor ( $M_{DEV}$ ), with  $M_{DEV}$  consisting of the DC and CLVD components:

$$M = M_{ISO} + M_{DEV} \quad (1)$$

$$M_{ISO} = \frac{1}{3} tr(M) \begin{bmatrix} 1 & 0 & 0 \\ 0 & 1 & 0 \\ 0 & 0 & 1 \end{bmatrix} \quad (2)$$

where  $tr(M)$  is the trace of the original moment tensor ( $M$ ) (Vavryčuk, 2015). This isotropic tensor represents the volumetric change of the source because it only consists of the double-couple forces along the diagonal of  $M$  (Dahm and Krüger, 2014). If the trace of  $M$  is zero, such as for pure DC sources, then the strength of the ISO mechanism of the source is zero.

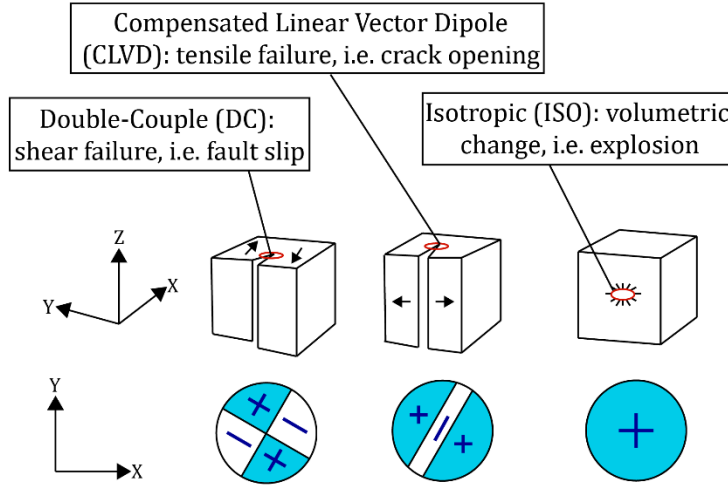


**Figure 2:** Failure mechanisms are represented on beach-ball diagrams (adapted from Baig and Urbancic (2010)). These diagrams indicate the directions in which the medium surrounding the source is moving such that the shaded (blue) areas of the beach-balls (+) represent the surrounding material moving away from the source whereas the non-shaded (white) areas (-) represent the surrounding material moving inward towards the origin of the source.

Moment tensors can imply three types of failure mechanisms: DC, CLVD, and ISO (Fig. 2). These mechanisms are visually represented on “beach-ball” diagrams, which are lower-hemisphere stereographic projections that represent the directions of motion at the source. The fault plane orientation (strike, dip, and rake) is interpreted from the beach-ball diagram ((Warpinski and Du, 2010). Sources can be interpreted as purely DC, CLVD, or ISO or they can be considered as a combination of the three failure mechanisms with different percentages of strength (i.e., 25% DC, 50% CLVD, 25% ISO).

The orientation and relative percentages of the DC and CLVD mechanisms of the source are determined from  $M_{DEV}$ . The eigenvector of  $M_{DEV}$  with the maximum eigenvalue represents the minimum compressional ( $\vec{T}$ ) axis of the source mechanism whereas the eigenvector of  $M_{DEV}$  with the minimum eigenvalue represents the maximum compressional ( $\vec{P}$ ) axis of the source mechanism (Song and Toksoz, 2011; Stein and Wyession, 2003) The  $\vec{T}$  and  $\vec{P}$  axes are related to the source orientation by

$$\vec{u} = \frac{1}{\sqrt{2}}(\vec{T} + \vec{P}) \text{ and } \vec{v} = \frac{1}{\sqrt{2}}(\vec{T} - \vec{P}) \quad (3)$$

where  $\vec{u}$  is the slip vector and  $\vec{v}$  is the fault plane normal (Jost and Hermann, 1989). We determine the strike  $\phi$ , dip  $\delta$ , and rake  $\lambda$  of the source using

$$\vec{u} = \begin{pmatrix} \cos \lambda \cos \phi + \sin \lambda \cos \delta \sin \phi \\ -\cos \lambda \sin \phi + \cos \lambda \cos \delta \cos \phi \\ \sin \lambda \sin \delta \end{pmatrix} \text{ and } \vec{v} = \begin{pmatrix} -\sin \delta \sin \phi \\ -\sin \delta \cos \phi \\ \cos \delta \end{pmatrix} \quad (4)$$

(Stein and Wyession, 2003).

Finally, the ratio of the CLVD component relative to the DC component is represented by the parameter  $\varepsilon$  and calculated from

$$\varepsilon = -\frac{e_{|min|}}{|e_{|max|}|} \quad (5)$$

where  $e_{|min|}$  and  $e_{|max|}$  are the minimum and maximum absolute eigenvalues of  $M_{DEV}$ , respectively (Song and Toksoz, 2011; Vavryčuk, 2001).

### Moment Tensor Inversion

The computational method of moment tensor inversion is the standard method for determining the source parameters of an earthquake from data recorded at a seismic receiver (Cronin, 2010). Moment tensor inversion solves for  $M$  (Eqn. 2) using input displacement data ( $u$ ) from seismic receivers and information (i.e. seismic velocities) about the Earth model ( $G$ ). The inversion problem is a least-squares fit of the minimization of the difference ( $\Delta$ ) between the input data ( $u_j$ ) and synthetic seismograms ( $a_n G_{jn}$ ):

$$\Delta = \sum_{j=1}^{N_s} \int \left[ u_j(t) - \sum_{n=1}^6 a_n G_{jn}(t) \right]^2 \quad (8)$$

where  $j$  is the  $j$ th receiver,  $N_s$  is the number of receivers, and  $a_n$  denotes the  $n$ th elementary seismogram representing the  $n$ th basic moment tensor (Table 1) (Kikuchi and Kanamori, 1991; Sokos and Zahradnik, 2008). The moment tensor is calculated with the six best-fit values of  $a_n$ , where  $a_n$  is the  $n$ th basic moment tensor. All possible moment tensors can be written as this combination of these six basic moment tensors (Sokos & Zahradnik, 2009), so that tensor  $M$  (Eqn. 2) can also be written as a combination of the six basic moment tensors (Warpinski & Du, 2010):

$$M = \begin{bmatrix} -a_5 + a_6 & a_1 & -a_3 \\ a_1 & -a_4 + a_6 & a_2 \\ -a_3 & a_2 & a_4 + a_5 + a_6 \end{bmatrix} \quad (6)$$

ISOLA (ISOLated Asperities) is a free and open-source moment tensor inversion program and graphical user interface that utilizes the full-wavefield in the Green's function (Sokos and Zahradnik, 2009). ISOLA is written in MATLAB© and Fortran 77 that simultaneously searches for the source location and mechanism of a seismic event (Sokos and Zahradnik, 2008). Whereas many other software assume pure shear sources associated with large-scale earthquakes and only solve for the orientation of the failure plane, ISOLA allows moment tensors to contain non-DC mechanisms (Hardebeck and Shearer, 2008; Sokos and Zahradnik, 2009). The source location, origin time, and moment tensor with the greatest correlation between the input and synthetic seismograms are the final output result from the inversion, along with other properties calculated from the moment tensor (Sokos and Zahradnik, 2009).

ISOLA also provides a deviatoric and a DC source-mechanism constraint (Sokos and Zahradnik, 2008). The deviatoric constraint assumes a negligible strength for the ISO source mechanism (0%) whereas the DC constraint assumes that the sources have a complete (100%) DC mechanism. When using the DC constraint, ISOLA first assumes a deviatoric constraint, then inverts while attempting to maximizing the DC percentage. If, within five iterations, no solution is found that has a DC contribution greater than 90%, as well as a good correlation to the input data, the original deviatoric result is output (Sokos and Zahradnik, 2008).

### Synthetic Seismogram Modeling

If we expand the formula for the Green's function  $G$  (Eqn. 1), the displacement  $u$  at receiver  $n$  at time  $t$  for an infinite, homogenous, and isotropic medium is:

$$\begin{aligned} u_n(x, t) = M_{pq} * G_{np,q} = & \left( \frac{15\gamma_n\gamma_p\gamma_q - 3\gamma_n\delta_{pq} - 3\gamma_p\delta_{nq} - 3\gamma_q\delta_{np}}{4\pi\rho} \right) \frac{1}{r^4} \int_{r/\alpha}^{r/\beta} \tau M_{pq}(t - \tau) d\tau \\ & + \left( \frac{6\gamma_n\gamma_p\gamma_q - \gamma_n\delta_{pq} - \gamma_p\delta_{nq} - \gamma_q\delta_{np}}{4\pi\rho\alpha^2} \right) \frac{1}{r^2} M_{pq} \left( t - \frac{r}{\alpha} \right) \\ & - \left( \frac{6\gamma_n\gamma_p\gamma_q - \gamma_n\delta_{pq} - \gamma_p\delta_{nq} - 2\gamma_q\delta_{np}}{4\pi\rho\beta^2} \right) \frac{1}{r^2} M_{pq} \left( t - \frac{r}{\beta} \right) \\ & + \frac{\gamma_n\gamma_p\gamma_q}{4\pi\rho\alpha^3} \frac{1}{r} \dot{M}_{pq} \left( t - \frac{r}{\alpha} \right) - \left( \frac{\gamma_n\gamma_p - \delta_{np}}{4\pi\rho\beta^3} \right) \gamma_q \frac{1}{r} \dot{M}_{pq} \left( t - \frac{r}{\beta} \right) \end{aligned} \quad (7)$$

where

$$\begin{aligned} \gamma_k &= k\text{th direction cosine between source and receiver} \\ \delta_{ab} &= \begin{cases} 0 & \text{if } a \neq b \\ 1 & \text{if } a = b \end{cases} \text{ (Kronecker delta)} \\ \rho &= \text{Density of medium} \\ r &= \text{Source-receiver distance} \\ \alpha &= \text{P-wave velocity of medium} \\ \beta &= \text{S-wave velocity of medium} \\ M_{pq} &= \text{Moment tensor (Aki and Richards, 2002)}. \end{aligned}$$

The first term represents the amplitudes of the near-field that decays at  $r^{-4}$  and has no distinguishable P- and S- wave arrivals (Aki and Richards, 2002). The second and third terms represent the intermediate-field amplitudes separated into P- and S-wave terms and decay at  $r^{-2}$ . The final two terms represent the far-field amplitudes with distinguishable P- and S-wave terms. The far-field amplitudes are what are mostly observed in earthquake data with large source-

receiver distances ( $> 1$  km) because of the low attenuation of  $r^{-1}$  (Aki and Richards, 2002). The intermediate- and near-field amplitudes are most apparent for source-receiver distances less than five times the S-wave wavelength because the amplitudes have not yet attenuated to negligible values and can contribute  $\sim 5$ -20% of the total wavefield. The source-time function  $s(t)$  is a Ricker wavelet calculated as

$$s(t) = (1 - 2\pi^2 f^2 t^2) e^{-\pi^2 f^2 t^2} \quad (18)$$

where  $f$  is the peak frequency (Ryan, 1994). The Ricker wavelet is commonly used for synthetic seismogram calculations because it is zero-phase and has only one input frequency which allows for a simple calculation (Ryan, 1994).

### Three Test Cases with Incorporation of Some Field Parameters

Input parameters for the synthetic seismogram calculation are selected to resemble values from a proprietary field case from a multi-stage field data set Barnett Shale of east Texas (Fig. 3a). The source-receiver geometry comprises a horizontal array of eight receivers and two treatment wells adjacent to a  $\sim$ NE-SW trending inactive fault zone (Fig. 3b). From this setting we choose three test locations where to conduct our error analysis (Fig. 4) each having different angular coverage and source-receiver distance: **1)** Location 1b has the lowest angular coverage ( $14^\circ$ ) and smallest average source-receiver distance ( $\sim 300$  m), **2)** location 3d has greater angular coverage ( $27^\circ$ ) and a larger source-receiver distance ( $\sim 325$  m) than 1b, and **3)** location 3d has the greatest angular coverage ( $32^\circ$ ) and the largest source-receiver distance ( $\sim 355$  m) (Fig. 4). Location 1b with the smallest source-receiver distance should have the greatest contribution of intermediate- and near-field terms ( $\sim 8\%$ ) to the total amplitude. We use one pure (100%) DC source, one pure CLVD source, and one pure ISO source in each test case to study the resolvability of the source components for different mechanisms. The DC and CLVD sources have an orientation consistent with the orientation in which vertical fractures open in the Barnett Shale during hydraulic fracturing (Gale et al., 2007)

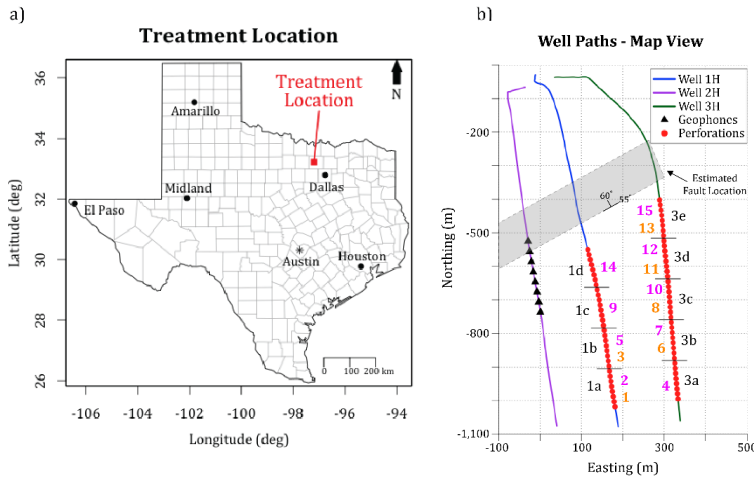


**Figure 3: a)** Map of Texas indicating the location of the hydraulic fracturing treatment in northeast Texas

**Figure 3: b)** Map view of well paths and locations of geophones in monitoring-well 2H and planned perforation locations for each stage for treatment-wells 1H and 3H. The black text labels indicate the treatment-well (1 or 3) and stage (a, b, etc.). The numbers in orange (perforation) and purple (treatment) indicate the order in which the perforations and treatment were completed, i.e. first stage 1a was perforated, then 1a was treated, then 1b was perforated, etc. The reference point of 0,0 is the XY surface location of well 1H. The gray box is the estimated location of a fault in this area

The isotropic velocity model uses an average  $V_p$  of 3.85 km/s and an average  $V_s$  of 2.37 km/s as determined from sonic logs. We use a one-layer velocity model and assume the sources and receivers are in the same layer to study the moment tensor inversion results with the simplest velocity model. The anisotropic case has a 5% VTI velocity model, in which the horizontal and vertical seismic velocities differ by up to 5%, to represent the low degree of anisotropy of the Barnett Shale (Song et al., 2014). To study the neglect of anisotropy in the moment tensor inversion, the synthetic seismogram calculation utilizes this anisotropic velocity model and the moment tensor inversion assumes an isotropic velocity model.

Three of the test cases are given a dominant source frequency of 125 Hz because of similarity to the frequency content of data from our field data and because microseismic events occurring during hydraulic fracturing treatments have generally been seen to also contain dominant source frequencies between 100 and 150 Hz (Eaton et al., 2013). We use two other dominant source frequencies of 50 Hz and 175 Hz to determine if events containing lower frequencies are more resolvable than events containing higher frequencies because events containing lower frequencies are expected to have less attenuated intermediate- and near-field seismogram amplitudes.

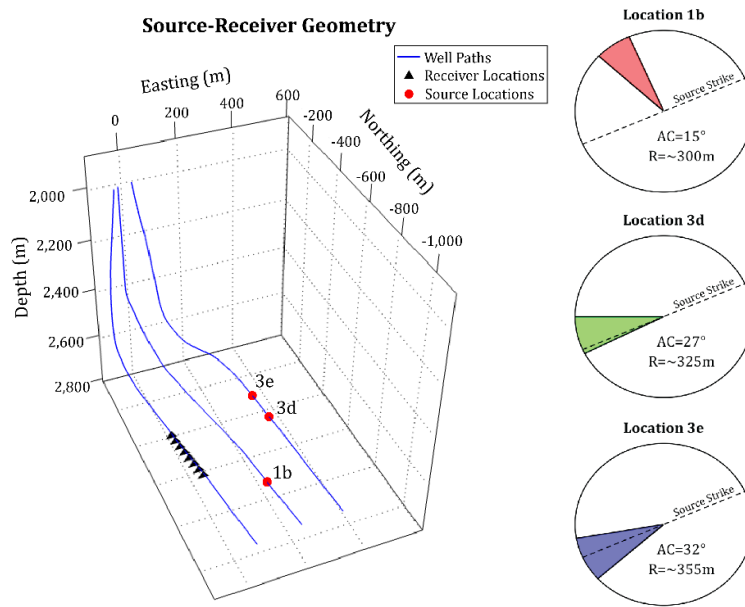


**Figure 4:** Oblique 3D view of source-receiver geometry used to calculate synthetic seismograms. There are eight receivers (black triangles) in a horizontal array approximately 300 m west of two of the test event locations (red circles): 3d and 3e. The third tested event location is at 1b. The origin 0,0,0 is taken as the surface location of the middle well. b) Pie charts showing receiver angular coverage of artificial events at locations 1b (top), 3d (middle), and 3e (bottom)

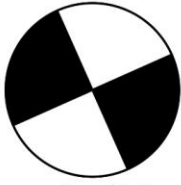
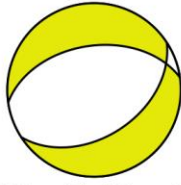
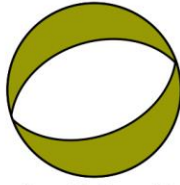
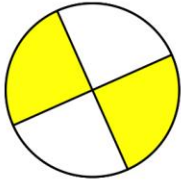
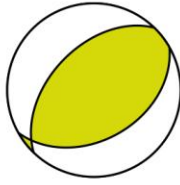
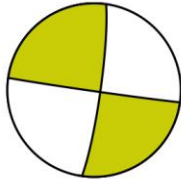
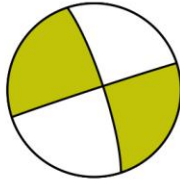
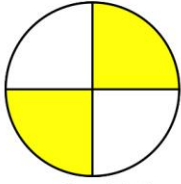
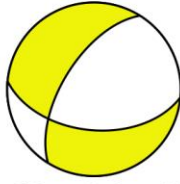
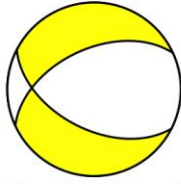
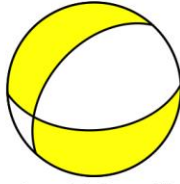
## Results

Those synthetic events with greater angular coverage ( $> 25^\circ$ ) have less error in the resolved source orientations ( $< 35^\circ$ ) than events with less angular coverage (Table; Fig. 5). This relationship is apparent regardless of event frequency, indicating that the resolvability of the source orientation is more dependent on receiver angular coverage (Fig. 5). However, it is also important to note the relationship between the expected source radiation pattern and receiver angular coverage (Fig. 6). The angular coverage of possible events at locations 3d and 3e provides sampling of both sides of potential fault planes such that both first-motion up and first-motion down P-wave polarities are detected at the receivers (Figs. 6b-c). The orientation of the focal mechanism is constrained using these P-wave polarities (Dahm and Krüger, 2014). The auxiliary plane is resolved for events at location 1b because of the symmetric radiation pattern of the DC source (Fig. 6a). When including the intermediate- and near-field terms in an unconstrained moment tensor inversion, the isotropic source has the least error ( $< 13\%$ ) in the resolved source mechanism because the least-squares minimization is finding a fit to a source with only P-wave amplitudes in the seismograms (Table).

### Angular Coverage and Deviatoric Constraints

We consider five scenarios to understand how angular coverage affects the results of full-wavefield moment tensor inversion:

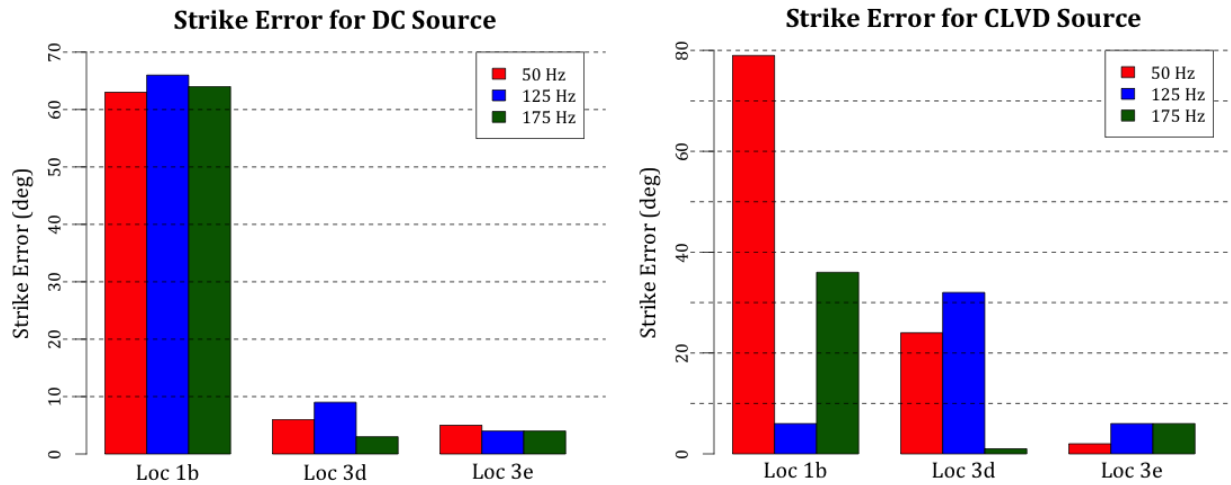
- 1) isotropic medium with dominant source frequency of 125 Hz
- 2) anisotropic (5% VTI) medium with dominant source frequency of 125 Hz:
- 3) isotropic medium with dominant source frequency of 125 Hz and 5% random Gaussian noise added to the seismograms
- 4) isotropic medium with dominant source frequency of 50 Hz
- 5) isotropic medium with dominant source frequency of 175 Hz.

Input	Output		
Beach-ball	Location 1b	Location 3d	Location 3e
DC=100% CLVD=0% ISO=0%  0 m E, 0 m N	DC=62% CLVD=22% ISO=16%  -25 m E, -25 m N	DC=9% CLVD=40% ISO=-51%  25 m E, -50 m N	DC=35% CLVD=42% ISO=-23%  0 m E, 0 m N
CLVD=100% DC=0% ISO=0%  0 m E, 0 m N	CLVD=1% DC=15% ISO=85%  25 m E, 50 m N	CLVD=11% DC=19% ISO=70%  25 m E, -50 m N	CLVD=15% DC=22% ISO=63%  0 m E, 0 m N
ISO=100% DC=0% CLVD=0%  0 m E, 0 m N	ISO=-87% DC=7% CLVD=6%  -50 m E, 0 m N	ISO=91% DC=2% CLVD=7%  25 m E, -50 m N	ISO=91% DC=2% CLVD=8%  0 m E, 0 m N

**Table 1:** Full-wavefield moment tensor inversion results of synthetic seismograms with pure DC (top row), pure CLVD (middle row), and pure ISO (bottom row) sources generated in an isotropic medium and with a dominant event frequency of 125 Hz. The first column shows the input mechanism. The coordinates below each beach-ball indicate the output location from ISOLA where 0 m E, 0 m N is the true source location. The second, third, and fourth columns represent sources occurring at locations 1b, 3d, and 3e, respectively and are in order of increasing angular coverage and decreasing source-receiver distance from left to right. No constraints on the source mechanism are applied to the inversion. The beach-balls are colored by the amount of the resolved DC mechanism such that 100% DC is black and 0% DC is yellow.

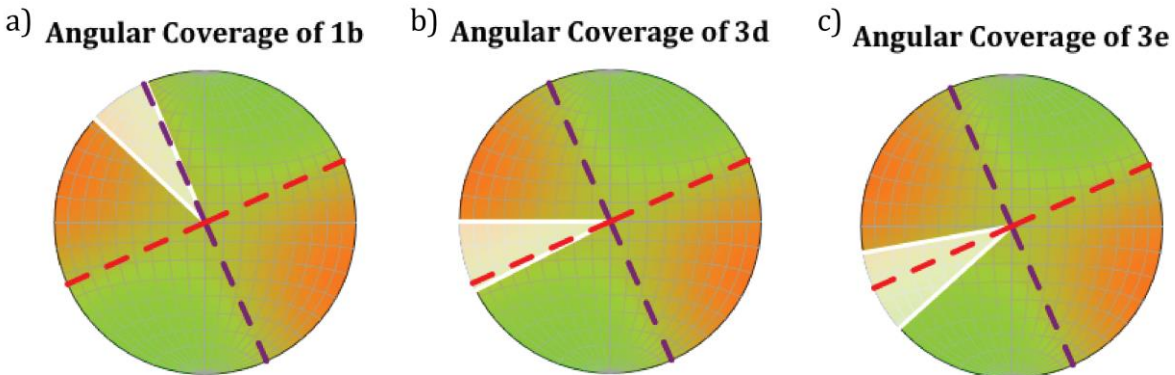
There is a relationship between the synthetic event location and angular coverage of the source such that location 3e with the greatest angular coverage always has the minimum location error of zero meters except in the anisotropy and low frequency cases (Fig. 7). Location 3d consistently has an error in location of approximately 50-55 m (Fig. 7) and has the moderate angular coverage of the three test locations. Location 1b, with the worst angular coverage, has the most varied error in location (~32-70 m) (Figure 7). Errors in the resolved failure show a sensitivity to the source-receiver distance and therefore highlight the importance using of the full-wavefield during moment tensor inversion.

When using full-wavefield moment tensor inversion and applying the deviatoric constraint, the results for CLVD sources with greater angular coverage ( $> 25^\circ$ ) have less error in the estimated source mechanisms than the DC sources (Table 2). The source orientation is accurately resolved for the CLVD source located closest to the receivers (location 1b) because of the inclusion of the intermediate- and near-field terms and correct application of the deviatoric constraint (Table 2-- top 2 rows). However, the other two locations (3d and 3e) have greater error in the source orientation with the deviatoric constraint applied than the results of the unconstrained full-wavefield moment tensor inversion (Table 2--bottom row).



**Figure 5:** Error in source strike from results of full-wavefield moment tensor inversion of synthetic seismograms for a) DC sources and b) CLVD sources. Sources with greater angular coverage (locations 3d and 3e) have less error in the resolved source strike than sources with less angular coverage (location 1b). This relationship is apparent in all three of the tested dominant source frequencies: 50 Hz (red), 125 Hz (blue), and 175 Hz (green).

For the ISO source, there is an appearance of non-DC components in the output results for the artificial events that have greater angular coverage ( $> 25^\circ$ ) with the DC constraint applied (Table 2--bottom row). On the other hand, the location with the least angular coverage (1b) resolves a dominantly DC source. The incorrect application of the DC constraint for moment of the DC constraint for moment tensor inversion of tensile sources results in greater error for sources with less angular coverage ( $14^\circ$ ) than for sources with greater angular coverage ( $> 25^\circ$ ). tensor inversion of tensile sources results in greater error for sources with less angular coverage ( $14^\circ$ ) than for sources with greater angular coverage ( $> 25^\circ$ ).

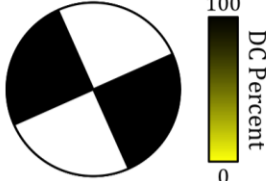
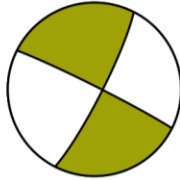
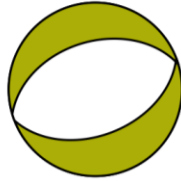
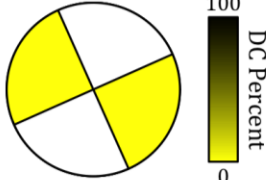
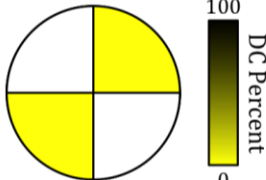
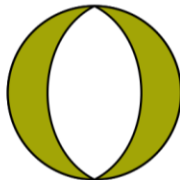
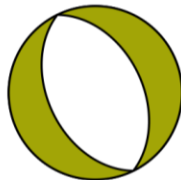


**Figure 6:** Lower-hemisphere stereographic projection of the P-wave radiation pattern of a DC source with strike of  $66^\circ$ , dip of  $90^\circ$ , and rake of  $0^\circ$  (dashed black line) with the angular coverage of the geophones (highlighted in white) relative to the source for an event at a) location 1b, b) location 3d, and c) location 3e. The auxiliary plane is perpendicular to the source orientation with a strike of  $156^\circ$  (purple dashed line). The orange areas represent the surrounding material moving outward from the source and the green areas represent the surrounding material moving inward to the source.

### Anisotropy

Moment tensor inversions are commonly used with only isotropic assumptions, however many geologic formations have anisotropic velocities (Thomsen, 1986). Shale is a vertically transverse isotropic (VTI) medium in which hydraulic fracturing is commonly completed in because of its low permeability (Maxwell and Norton, 2012). In VTI media, the seismic velocities vary vertically as a function of the angle between the vertical axis and the direction of wave propagation (Ikelle and Amundsen, 2005; Thomsen, 1986). When inverting events with waveforms generated in anisotropic media but assuming isotropy, the error in the resolved source orientation is low ( $< 20^\circ$ ), however, the CLVD and ISO components are overestimated for pure-DC sources (Sileny and Vavryčuk, 2002).

The majority of the full-wavefield moment tensor inversion results in the entire grid search have less than a 15° difference in the resolved source strike between the isotropic and anisotropic cases (Fig. 8). On the other hand, the resolved strength of the DC mechanism has a greater difference of ~25%. These differences indicate that the neglect of anisotropy in the velocity model for moment tensor inversion introduces greater variation in the resolved source mechanism than the resolved source orientation (Fig. 8). (The addition of 5% random Gaussian noise to the seismograms does not significantly alter the results of full-wavefield moment tensor inversion from that of the results of the noise-free seismograms).

Input	Output		
Beach-ball	Location 1b	Location 3d	Location 3e
DC=100% CLVD=0% ISO=0%  0 m E, 0 m N	DC=87% CLVD=13% ISO=0%  -25 m E, -25 m N	DC=32% CLVD=68% ISO=0%  25 m E, -50 m N	DC=28% CLVD=72% ISO=0%  0 m E, 0 m N
CLVD=100% DC=0% ISO=0%  0 m E, 0 m N	CLVD=15% DC=85% ISO=0%  -25 m E, -25 m N	CLVD=40% DC=60% ISO=0%  25 m E, -50 m N	CLVD=52% DC=48% ISO=0%  0 m E, 0 m N
ISO=100% DC=0% CLVD=0%  0 m E, 0 m N	ISO=0% DC=99% CLVD=1%  -50 m E, 50 m N	ISO=0% DC=31% CLVD=69%  25 m E, -50 m N	ISO=0% DC=32% CLVD=68%  0 m E, 0 m N

**Table 2: Results From Application of Deviatoric and DC Constraints.** Full-wavefield moment tensor inversion results of synthetic seismograms with pure DC (top row) a pure CLVD (second row) and a pure ISO source (bottom row) generated in an isotropic medium and with a dominant event frequency of 125 Hz. The first column shows the input mechanism. The coordinates below each beach-ball indicate the output location from ISOLA where 0 m E, 0 m N is the relative, true source location. The second, third, and fourth columns represent sources occurring at locations 1b, 3d, and 3e, respectively and are in order of increasing angular coverage and decreasing source-receiver distance from left to right. For the first two rows, a deviatoric constraint in which the ISO component is assumed to be 0% is applied to the inversion. For the bottom row, a DC constraint in which both the CLVD and ISO components are assumed to be 0% is applied to the inversion. The beach-balls are colored by the amount of the resolved DC mechanism such that 100% DC is black and 0% DC is yellow.

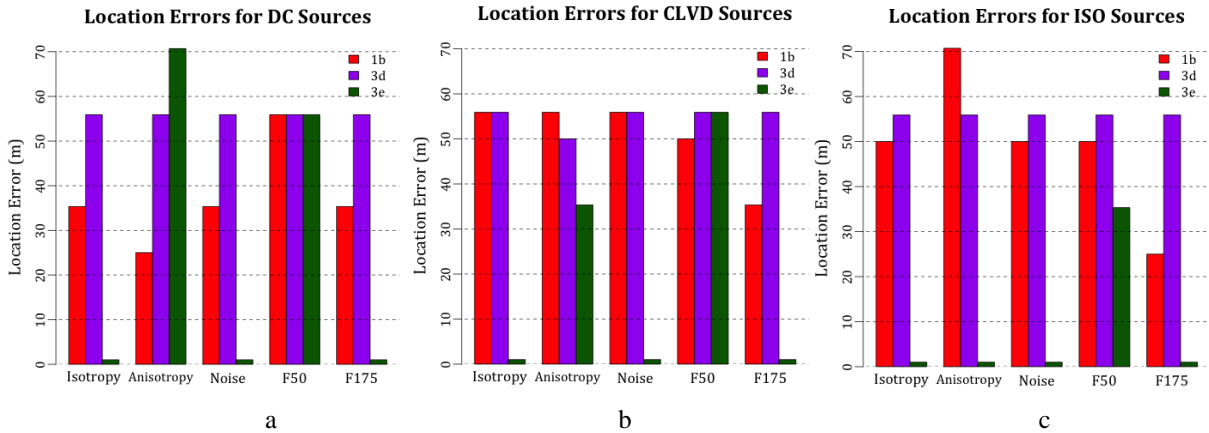


**Figure 7 : Location Error Bar Plots** for a) DC sources, b) CLVD sources, and c) ISO sources. The five different test cases are plotted along the x-axis in order of: isotropy, anisotropy, noise, frequency of 50 Hz, and frequency of 175 Hz. Each case is separated into three different bars representing each location: 1b (red), 3d (purple), and 3e (green).

**Discussion**

Previous studies of moment tensor inversion with only consideration of the far-field terms show that the pure shear source is the most accurate to retrieve from microseismic data from a single vertical array of receivers when applying a deviatoric constraint to the inversion (Vavryčuk, 2007; Warpinski and Du, 2010). When including the intermediate- and near-field terms and applying no source constraints, the calculated mechanism percentages are

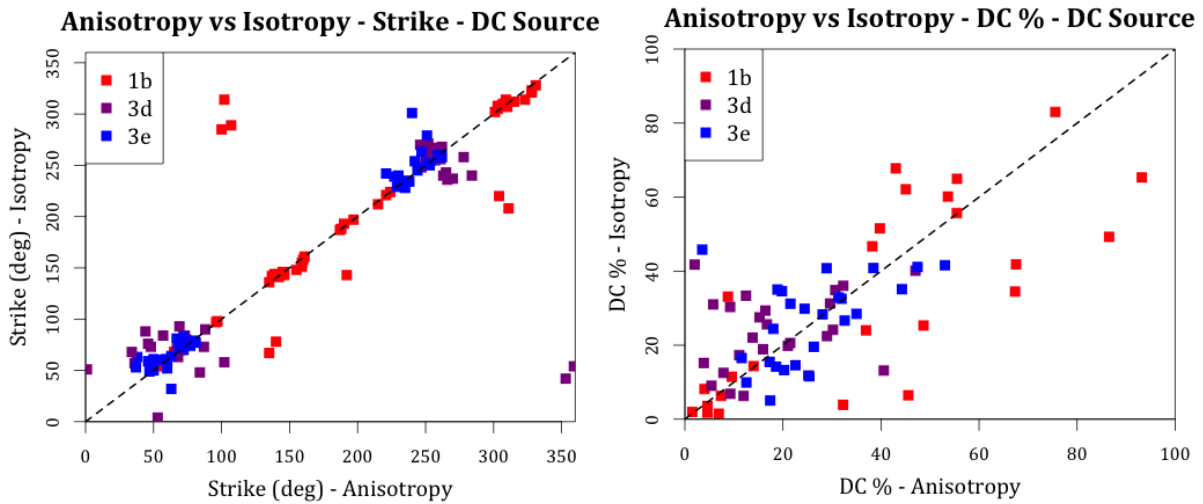


**Figure 8:** Comparison of full-wavefield moment tensor inversion (assumes isotropic seismic velocities) results for sources occurring in anisotropic (x-axes) and isotropic (y-axes) media. a) Comparison of the strike of the DC source shows little variability ( $< 15^\circ$ ) for all locations in the grid search. b) Comparison of the strength of the resolved DC mechanism shows greater variability ( $\sim 25\%$ ). These results indicate that the neglect of anisotropy in the velocity model has a greater effect on the resolved mechanism percentages than the resolved source orientation. The dash blacked line is the line with the equation  $x=y$ .

more accurate for pure shear sources located closer to a horizontal receiver array than sources located farther from the receiver array.

A preliminary understanding of the relationship between receiver angular coverage and the expected source radiation pattern should be considered when interpreting the results of moment tensor inversion. Sources that do not have receiver angular coverage of both sides of the shear failure plane will not be able to resolve the correct orientation fully. This is important for moment tensor inversion programs that apply a constraint on the source orientation to reduce the error in the results associated with lack of angular coverage (Song and Toksoz, 2011).

Applying the source orientation constraint without receiver angular coverage of both sides of the failure plane could introduce greater error into the estimated source mechanism than the results without the constraint.

### **Deviatoric Constraint**

The resolved strength of the shearing mechanism is greater for results of full-wavefield moment tensor inversion with the deviatoric constraint applied than when the inversion is unconstrained, for both shear and tensile sources (Table 2). If the source is dominantly shear, the deviatoric constraint decreases the error in the source mechanism but increases the error in the source orientation. The introduction of these secondary errors indicates that, without prior knowledge of whether the source is dominantly shear or tensile, the deviatoric constraint should not be used to stabilize the inversion of sources with limited angular coverage. The results of unconstrained full-wavefield moment tensor inversion can be interpreted with an understanding of the errors associated with the lack of angular coverage rather than adding possible additional error with the use of the deviatoric constraint.

### **Neglect of Anisotropy in Moment Tensor Inversion**

The effects of anisotropic velocities on moment tensor inversions that assume isotropic velocity models are well studied for shear sources but limited work is done for non-DC sources (Röbber et al., 2007; Sileny and Vavryčuk, 2002; Vavryčuk, 2005). A previous study shows that the CLVD mechanism can be overestimated by ~20% more than the ISO mechanism for pure shear sources when neglecting anisotropy in the moment tensor inversion (Sileny and Vavryčuk, 2002). Inversion of synthetic seismograms in ISOLA, which utilizes an isotropic velocity model, shows that the difference between the resolved source mechanism of sources generated in an isotropic medium and the resolved source mechanism of sources generated in a 5% VTI medium is ~40% greater for CLVD sources than DC sources (Fig. 8). If CLVD source mechanisms are expected, an understanding of both the errors that the neglect of anisotropy introduces into the results of moment tensor inversion and the errors associated with the lack of angular coverage should be considered in the interpretation of the results.

Previous studies suggest using only the P-wave amplitudes in the moment tensor inversion to mitigate the effect of anisotropy on S-wave splitting (Sileny and Vavryčuk, 2002). However, Vavryčuk (2007) shows that sufficient angular coverage of at least two non-parallel receiver arrays (i.e. one vertical and one horizontal) is required for moment tensor inversion using only the P-wave amplitudes and far-field terms of the wavefield. More work on full-wavefield moment tensor inversion with only use of the P-wave amplitudes is needed to determine if a single array of receivers located close (< 300 m) to the source can provide accurate source mechanisms.

### **Conclusions**

Based on full-wavefield moment tensor inversion (ISOLA open source software) of synthetic seismograms representing pre-determined pure DC and CLVD events, the source mechanism and orientation cannot be determined when using a single-horizontal array of receivers. Future studies utilizing moment tensor inversion of microseismic data should consider the receiver angular coverage of the events being inverted to determine if the source mechanisms can be accurately resolved.

Several relationships between receiver angular coverage of the source and the full-wavefield moment tensor inversion stand out. First is the relationship with the resolvability of the source orientation. The strike of shear sources cannot be accurately resolved unless there is receiver angular coverage of both sides of the failure plane. The second relationship is with the error in source location such that sources with less angular coverage have greater error in source location. Moment tensor inversion results at all locations in the grid search show minimal variability between locations. This lack of variability indicates that the errors in the inversion results are mainly because of the lack of the angular coverage of the source rather than the source mislocation.

For moment tensor inversion of pure shear sources generated in a 5% VTI medium, we show that there is greater variability in the resolved source mechanism than the source orientation compared to the pure shear sources generated in an isotropic medium. The use of an isotropic velocity model for events occurring in an anisotropic medium can introduce a 25-50 m error into the estimation of the source location.

Hydraulic fracturing treatments in complex geologic settings, such as the one presented here where the formation has natural fractures and a nearby fault, should consider what microseismic event characteristics are desired when designing the microseismic monitoring survey. With sufficient angular coverage, accurate source mechanisms can

be retrieved to understand the interaction between the hydraulic fractures, fault, and natural fractures. To take advantage of the full-wavefield, receivers should be placed as close to the treatment area as possible and with more geophones and/or a wider spacing of geophones than the design of the horizontal array considered herein. The synthetic seismograms are constructed using similar to the estimated locations and dominant frequencies of the events in the provided microseismic data, indicating that full-wavefield moment tensor inversion cannot be used to retrieve accurate source mechanisms for these events.

### Acknowledgements

We thank Schlumberger for providing the original microseismic data. Initial work on these data was made possible through a Louisiana Board of Regents Grant to the first and last author during 2011-13.

### References

- Aki, K., Richards, P.G., 2002. Quantitative Seismology. University Science Books, Sausalito, CA.
- Baig, A., Urbancic, T., 2010. Microseismic moment tensors: A path to understanding frac growth. *The Leading Edge* 29, 320-324.
- Bormann, P., Wendt, S., Giacomo, D.D., 2013. Seismic Sources and Source Parameters, *New Manual of Seismological Observatory Practice*.
- Cronin, V., 2010. A Primer on Focal Mechanism Solutions for Geologists.
- Dahm, T., Krüger, F., 2014. Moment tensor inversion and moment tensor interpretation, in: Bormann, P. (Ed.), *New Manual of Seismological Observatory Practice 2 (NMSOP-2)*, Potsdam : Deutsches GeoForschungsZentrum GFZ, pp. 1-37.
- Eaton, Baan, M.v.d., Tary, J.-B., Birkelo, B., Spriggs, N., Cutten, S., Pike, K., 2013. Broadband microseismic observations from a Montney hydraulic fracture treatment, northeastern B.C., Canada. *CSEG Recorder*, 44-53.
- Eisner, L., Fischer, T., Calvez, J.H.L., 2006. Detection of repeated hydraulic fracturing (out-of-zone growth) by microseismic monitoring. *The Leading Edge*.
- Forouhideh, F., Eaton, D.W., 2009. Microseismic Monitoring: Insights from Moment Tensor Inversion. CREWES Research Report.
- Gale, J.F.W., Reed, R.M., Holder, J., 2007. Natural fractures in the Barnett Shale and their importance for hydraulic fracture treatments. *AAPG Bulletin* 91, 603-622.
- Hardebeck, J.L., Shearer, P.M., 2008. HASH: A FORTRAN Program for Computing Earthquake First-Motion Focal Mechanisms - v1.2 - January 31, 2008.
- Ikelle, Amundsen, 2005. Introduction to Petroleum Seismology.
- Jost, M.L., Hermann, R.B., 1989. A Student's Guide to and Review of Moment Tensors. *Seismological Research Letters* 60, 37-57.
- Kikuchi, M., Kanamori, H., 1991. Inversion of Complex Body Waves-III. *Bulletin of the Seismological Society of America* 81, 2335-2350.
- Maxwell, S., Norton, M., 2012. Enhancing shale gas reservoir characterization using hydraulic fracture microseismic data. *First Break* 30, 95-101.
- Röbller, D., Krüger, F., Rumpker, G., 2007. Retrieval of moment tensors due to dislocation point sources in anisotropic media using standard techniques. *Geophysical Journal International* 169, 136-148.
- Ryan, H., 1994. Ricker, Ormsby, Klauder, Butterworth - A Choice of Wavelets. *CSEG Recorder*.
- Sileny, J., Vavryčuk, V., 2002. Can unbiased source be retrieved from anisotropic waveforms by using an isotropic model of the medium? *Tectonophysics* 356, 125-138.
- Sokos, Zahradnik, J., 2008. ISOLA a Fortran code and a Matlab GUI to perform multiple-point source inversion of seismic data. *Computers & Geosciences* 34, 967-977.
- Sokos, Zahradnik, J., 2009. A Matlab GUI for use with ISOLA Fortran: User's Guide.
- Song, F., Toksoz, M.N., 2011. Full-waveform based complete moment tensor inversion and source parameter estimation from downhole microseismic data for hydrofracture monitoring. *Geophysics* 76, WC103-WC116.
- Song, F., Warpinski, N.R., Toksoz, M.N., 2014. Full-waveform based microseismic source mechanism studies in the Barnett Shale: Linking microseismicity to reservoir geomechanics. *Geophysics* 79, B109-B126.
- Stein, S., Wysession, M., 2003. *An Introduction to Seismology, Earthquakes, and Earth Structure*. Blackwell, Malden, MA.
- Thomsen, L., 1986. Weak elastic anisotropy. *Geophysics* 51, 1954-1966.

- Urbancic, T., Morrish, T., Shumila, V., 2009. Understanding Hydraulic Fracture Growth by Mapping Source Failure Mechanisms, Frontiers + Innovation CSPG CSEG CWLS Convention, Alberta, Canada.
- van der Baan, M., Eaton, D., Dusseault, M., 2013. Microseismic Monitoring Developments in Hydraulic Fracture Stimulation.
- Vavryčuk, V., 2001. Inversion for parameters of tensile earthquakes. *Journal of Geophysical Research* 106, 16339.
- Vavryčuk, V., 2005. Focal mechanisms in anisotropic media. *Geophysical Journal International* 161, 334-346.
- Vavryčuk, V., 2007. On the retrieval of moment tensors from borehole data. *Geophysical Prospecting* 55, 381-391.
- Vavryčuk, V., 2015. Moment Tensors: Decomposition and Visualization. 1-16.
- Warpinski, N.R., Du, J., 2010. Source-Mechanism Studies on Microseismicity Induced by Hydraulic Fracturing, Society of Petroleum Engineers Annual Technical Conference and Exhibition, Florence, Italy, 19-22 September 2010.
- Warpinski, N.R., Waltman, C.K., Du, J., Ma, Q., 2009. Anisotropy Effects in Microseismic Monitoring, Society of Petroleum Engineers Annual Technical Conference and Exhibition, New Orleans, Louisiana, USA, 4-7 October, 2009.